



Inherent strain approach to estimate residual stress and deformation in the laser powder bed fusion process for metal additive manufacturing—a state-of-the-art review

Hossein Mohammadtaheri¹ · Ramin Sedaghati · Marjan Molavi-Zarandi²

Received: 26 May 2022 / Accepted: 26 August 2022 / Published online: 8 September 2022
© The Author(s), under exclusive licence to Springer-Verlag London Ltd., part of Springer Nature 2022

Abstract

In recent years, metal additive manufacturing (AM) and particularly the laser powder bed fusion (LPBF) process have substantially grown in popularity in industrial applications due to its unique ability to produce a wide variety of components with complex geometry. The LPBF process is now an integral part of digital manufacturing and the industry 4.0 concept. However, a considerable amount of residual stress and deformation induced by the fast and intense heating/cooling cycle as well as phase change in each layer are still some important technical barriers in the LPBF process, giving rise to increasing inaccuracy and structural failure in some cases. Developing an efficient physics-based simulation model capable of predicting the induced residual stresses is, thus, of paramount importance to build parts with minimal distortion in a wide range of applications, while avoiding expensive and time-consuming experimental procedures. The simulation model also is efficiently utilized to investigate the effect of process parameters, material, and geometry on the development and redesign of parts. In the last decade, multi-scale process modeling frameworks have been developed to predict the residual stress and deformation cost-effectively in the parts fabricated by LPBF. The purpose of this survey is to systematically provide an in-depth overview of the inherent strain modeling approach with a focus more on the methodology development, highlighting the positive outcomes and limitations of recent investigations, followed by presenting potential future work to optimize this technique.

Keywords Metal additive manufacturing · Laser powder bed fusion · Inherent strain method · Finite element method

1 Introduction

In the past decade, the versatile metal laser powder bed fusion (LPBF) has been recognized as an accepted method for the fabrication of complex-shaped prototypes with excellent resolution, high performance, reduced material waste, and dramatically shortened time between design and

manufacture [1, 2]. Despite these superior properties, many applications in the biomedical, aerospace, and automotive industries are affected by several restrictions and technical barriers, ranging from porosity defects, micro-cracks, and balling effect to warping and distortion related to large temperature gradients experienced in the LPBF process [3–8]. Typically, the LPBF utilizes a high-density laser beam as a thermal source to selectively melt the materials in the form of powder onto a build plate along a pre-defined scanning route in a layer upon layer fashion. Deposited layers are fused together based on the sliced layer geometry until the desired shape is entirely built. Due to a high magnitude of temperature gradient, phase change transformation, and fast thermal and cooling cycles, a significant amount of residual stress is created, and subsequent deformation occurs in the components [9–11]. Although many experimental investigations using X-ray diffraction, hole drilling, contour method, and laser line profilometry have been conducted to study the influence of different process parameters on residual stress formation [12–21], these experiments are not only often very

✉ Hossein Mohammadtaheri
hossein.mohammadtaheri@concordia.ca

Ramin Sedaghati
ramin.sedaghati@concordia.ca

Marjan Molavi-Zarandi
marjan.molavi-zarandi@cnrc-nrc.gc.ca

¹ Department of Mechanical, Industrial & Aerospace Engineering, Concordia University, Montreal, QC H3G 2W1, Canada

² National Research Council Canada (NRC), 75 Boulevard de Mortagne, Boucherville, QC J4B 6Y4, Canada

costly and time-consuming, but they cannot also explicitly demonstrate how the temperature and thermal stress fields evolve over time. For instance, Kantzos et al. [22] examined the effects of beam power, scan speed, and hatch spacing alterations on the microstructures and mechanical properties of Inconel 718. Young et al. [23] determined the characteristics and propagation mechanisms of five principal forms of spatter during the LPBF process by using in situ high-speed, high-energy X-ray imaging. Gockel et al. [24] proposed a method to determine the relationship between surface roughness and laser power and speed and fatigue performance of alloy 718. Nayak et al. [25] successfully achieved the LPBF of a dense IN625 at a higher layer thickness of 100 μm by varying the combined parameters of laser energy density. Obviously, the LPBF process is affected by several contributing factors, such as material types, process parameters, and the geometry of the part. The examination of the effect of these factors on the induced thermo-mechanical residual stresses and distortion experimentally would be impractical if not impossible. Although experimental validation is still necessary, a reliable numerical modeling may significantly reduce the number of costly experimental trials in some certain conditions. Therefore, numerical-based techniques have emerged as promising tools to fundamentally understand the multiple highly coupled thermophysical phenomenon occurring during the LPBF process and to systematically investigate the effect of process parameters, material, and geometry factors on the induced residual stresses and part defects. The validated high fidelity numerical simulation model can be effectively utilized to accurately and efficiently predict the temperature distribution, induced residual stresses, and distortion in the entire parts under varied process parameters and part's geometry and material factors without carrying out time-consuming and expensive trial and error experiments.

In the LPBF process modeling, a significant amount of computational effort is required due to highly non-linear plastic deformation, transient heat transfer, fluid dynamics, and chemical reactions within the melt pool [26]. One of the major challenging issues in the simulation and modeling of LPBF is taking into consideration all complex multi-physics, namely, phase change transformation from solid to liquid, wetting and capillary forces, Marangoni convection phenomenon, recoil pressure, surface tension, and vaporization [27]. As a result, considering all the complex multi-physics in modeling leads to increasing computational time significantly for solving the problem. Because fluid dynamics equations and chemical reactions have negligible effects, they are frequently ignored in many studies focusing on residual stress and deformation prediction [28, 29]. Induced residual stresses and deformation have been initially predicted by the detailed thermo-mechanical simulations using a thermal source model [30–37]. However, despite its high

accuracy, due to an infinitesimal laser spot size and thousands of thin layers with a thickness at the micron level, the LPBF detailed thermo-mechanical simulation for the complex geometric parts requires a large number of time steps to estimate residual stress and deformation, which is not computationally cost-effective. Furthermore, based on the large thermal gradient near the heat source, the mesh size must be sufficiently small to accurately predict the induced residual stress and deformation of the deposited layers in the heat-affected zone. Therefore, applying a coupled thermo-mechanical analysis for multiple laser scans with a fine mesh model to macro-scale simulation would incur excessively large computational costs. Additionally, the large number of degrees of freedom for each element in the mechanical analysis leads to higher complexity as well as a longer amount of processing time. Detailed thermo-mechanical analysis for an industrial component is almost impractical since it would demand hundreds of terabytes of memory and years to calculate. Although many simplified strategies, such as the layer lumping method [38–41], static and dynamic adaptive mesh refinement techniques [33, 42–47], multi-scale modeling framework [6, 38, 41], and simplified heat source modeling and heat transfer problems [48, 49], have been developed over years to improve the efficiency of LPBF simulation with reasonable accuracy, the computational time has not been significantly improved, particularly for complicated industrial components. To overcome the huge computational burden associated with the numerical simulation of LPBF process, a number of studies have been conducted to explore the inherent strain method (ISM) proposed by Ueda [50, 51] as the most viable and efficient approach to predict the induced residual stress in the welded parts. Furthermore, the applied plastic strain method inspired by the inherent strain theory was developed to predict the residual distortion of laser engineered net shaping process [52, 53]. Both the suggested methods led to reducing the calculation time significantly. Since the numerical simulation of PBF is almost similar to the multi-pass welding process, the extension of the ISM in AM parts was drawn remarkable interest [54]. The possibility of applying this well-established method in AM was comprehensively investigated, demonstrating that the computational cost may be decreased from potentially days or weeks to a few hours while maintaining the accuracy compared to the detailed thermo-mechanical simulation [49, 55, 56]. Although the ISM has been introduced in many commercial software packages such as Abaqus [57, 58], MSC Simufact [10], Autodesk Netfabb [45], and Ansys [58, 59] for industrial parts simulation, their underlying algorithms (i.e., how the inherent strains are extracted and applied to the part-scale model) are not described in detail.

This paper attempts to provide a comprehensive overview of finite element-based modeling of the LPBF process using the inherent strain approach. In Sect. 2, an explanation of

fully and partially coupled thermo-mechanical simulation involving their governing equations is presented. Furthermore, it summarizes the articles that discussed the classical inherent strain theory, based on the physical phenomenon in the welding process. In Sect. 3, a detailed description of thermal and mechanical simulations at the multi-scale framework using the modified inherent strain method (MISM) is presented. In Sect. 4, the practical implications of the research associated with the ISM are reviewed. Finally, the conclusion and some future research possibilities are provided.

2 Thermo-mechanical simulations

The detailed thermo-mechanical simulation is divided into fully coupled and partially coupled techniques. The fully coupled method considers the thermal and mechanical analyses consecutively in which the temperature field is affected by modified geometry in every increment. The partially coupled method, on the other hand, utilizes the temperature history derived from a complete transient thermal analysis as a thermal load to be used in structural analysis separately [60]. Due to the poor coupling between the mechanical and thermal fields in the LPBF process and also computational efficiency, the majority of research studies are based on the partially coupled approach [11]. In this section, the governing equations for the detailed thermo-mechanical simulations are provided in order to have a better understanding of their differences and implementation of the finite element method based on these approaches. In addition, following the explanation of the classical inherent strain theory as an efficient alternative numerical method in welding and AM simulations, some of the associated improvements and validations are discussed.

2.1 Fully coupled approach

The typical flow chart for the fully coupled modeling of temperature and thermal stress fields in the LPBF process is illustrated in Fig. 1 [61]. The coupled temperature-displacement analysis is performed sequentially from the

bottom layer to the final top layer, wherein each layer, it is conducted on every increment of each scanning track. In the early stage of the analysis, which is done on the first scanning track of the substrate, since the displacement is zero, the temperature field extracted from the thermal analysis in the first increment is applied as a load to determine the displacement value for the next increment. This procedure continues increment by increment from each layer to another layer, until the last increment in the final scanning track of the top layer is being analyzed. As a consequence, the residual stress and deformation of the built part can be predicted.

The governing heat transfer energy equation of coupled thermoelectricity for temperature distribution can be written as follows [62]:

$$kT_{,ii} - \rho c \dot{T} - \alpha T_0 (3\lambda + 2\mu) \dot{\epsilon}_{ii} + Q = 0 \tag{1}$$

where ρ is the material density, c is the temperature-dependent heat capacity, T is the temperature, k is the temperature-dependent thermal conductivity of the material, λ and μ are the Lamé elastic constants, α is the coefficient of thermal expansion, T_0 is the reference temperature, ϵ is the strain, and Q rate is defined by the heat generated within the body per unit volume and unit time. As can be seen in the fully coupled approach, the governing transient heat transfer equation for temperature variation includes the rate of strain.

The governing equation for displacement can be derived by combining the equations of motion, strain–displacement relations, and constitutive Hook’s law equation stated as [62, 63]:

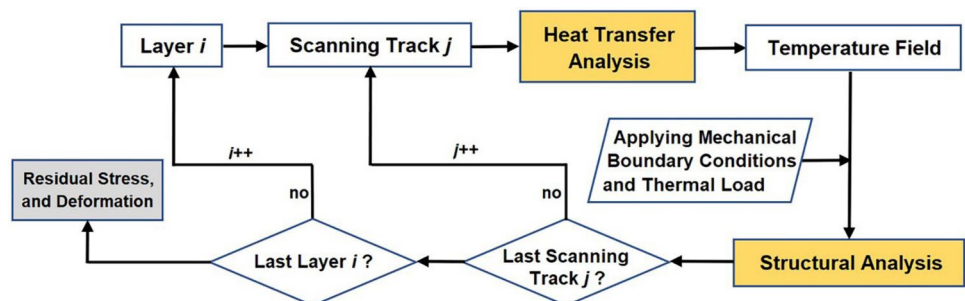
$$\text{Equations of motion : } \sigma_{ij,j} = \rho \ddot{u}_i \tag{2}$$

$$\text{Strain-displacement relations : } \epsilon_{ij} = \frac{1}{2}(u_{i,j} + u_{j,i}) \tag{3}$$

$$\text{Constitutive equations : } \sigma_{ij} = 2\mu \epsilon_{ij} + \lambda \epsilon_{kk} \delta_{ij} - (3\lambda + 2\mu) \alpha (T - T_0) \delta_{ij} \tag{4}$$

Substituting Eq. (3) for strains into Eq. (4) and then substituting the resultant into Eq. (2) yields the following governing equation for displacement:

Fig. 1 Flowchart of fully coupled thermo-mechanical FE model [61]



$$\mu \nabla^2 u_i + (\lambda + \mu) u_{k,ki} - \alpha(3\lambda + 2\mu)(T - T_0)_{,i} + F_i = 0 \quad (5)$$

where F_i is the body force per unit volume and δ_{ij} denotes the Kronecker’s symbol expressed by:

$$\delta_{ij} = \begin{cases} 1 & \text{for } i = j \\ 0 & \text{for } i \neq j \end{cases} \quad (6)$$

Equations (1) and (5) are fully coupled with respect to both temperature and displacement. These coupled equations together with initial and boundary conditions for thermal and mechanical loads can provide the displacement and temperature distribution in a part.

2.2 Partially coupled approach

In the partially coupled simulation, a thorough thermal analysis for the given geometry and boundary conditions is performed first, and the resultant temperature history is implemented as thermal loads in the quasi-static mechanical analysis. Therefore, the thermal and mechanical governing equations are independent (Fig. 2). The energy Eq. (1) is simplified to a 3D heat transfer Fourier equation for homogeneous isotropic materials to obtain the transient temperature distribution as follows:

$$kT_{,ii} - \rho c \dot{T} + Q = 0 \quad (7)$$

In mechanical analysis, the material constitutive model can be assumed to be either elastic and perfectly plastic with the $J2$ -von Mises plasticity law [10, 64] or pure plastic behavior with isotropic/kinematic or mixed strain hardening rules, using the associative $J2$ plasticity law [65, 66].

$$\sigma = C : \epsilon_e \quad (8)$$

$$\epsilon_{total} = \epsilon_e + \epsilon_p + \epsilon_{th} \quad (9)$$

$$\epsilon_{th} = \alpha \cdot \Delta T \quad (10)$$

$$f_{yield} = \sigma_m - \sigma_Y = 0 \quad (11)$$

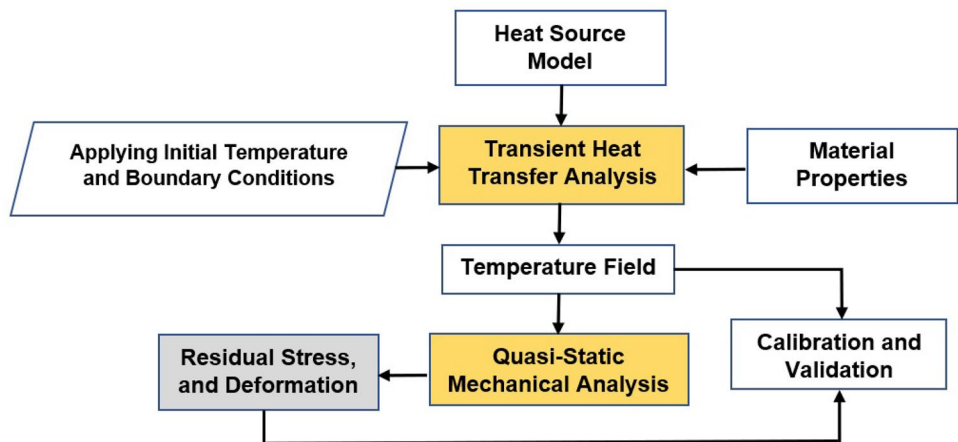
where C is the fourth-order material stiffness tensor; $\epsilon_e, \epsilon_p, \epsilon_{th}$ are the second-order elastic, plastic, and thermal strain tensors, respectively; α is the temperature-dependent coefficients of thermal expansion; and ΔT represents the temperature change during the process. σ_m is the von Mises stress, and σ_Y is the yield stress determined by the uniaxial tensile test. To consider the strain hardening rules, σ_Y can also be expressed by the Johnson–Cook plasticity model [67]. Typically, it is assumed that the plastic strain occurs for $f_{yield} > 0$.

2.3 Original inherent strain method (ISM)

Based on the proposed method by Ueda [50, 51], the inherent strain method involves two main steps: (1) conducting a detailed thermo-mechanical simulation on a micro-scale specimen to compute the plastic strain tensor once the built part cools down to room temperature and (2) applying the resultant plastic strain tensor to an actual component and performing a linear elastic analysis. In computational welding mechanics, the micro-welding process involves rapid heating, melting, and cooling cycles of the material along the weld line, which results in a significant temperature gradient and residual deformation [68]. Therefore, the total strain throughout the process is constituted by the summation of elastic, plastic, thermal, and phase change strains. The original inherent strain theory assumes that the total elastic strain is relieved after the welded part is cooled down to ambient temperature. Moreover, considering the final cooled state of the part, the thermal strain vanishes. Thus, by neglecting the infinitesimal phase change strain for the simplification [51], the inherent strain equals the plastic strain formed during the welding process.

Keller and Ploshikhin [55] applied the inherent strain theory in a new multi-scale approach to the AM process for

Fig. 2 Flowchart of partially coupled thermo-mechanical FE model



the first time to approximate the deformation and residual stress distribution. They proposed three models at different lengths and time scales to account for both thermal and mechanical development during the LPBF process, namely, micro-scale calibration of a heat source model, meso-scale analysis of the hatching strategy to extract the inherent strains, and macro-scale development of a mechanical layer equivalent (MLE) model. The small-scale modeling includes laser power, scanning speed, hatching pattern, and layer thickness as the main process parameters. The computed inherent strains obtained from the meso-scale are then loaded onto a macro-scale finite element model as the initial strains to predict the residual stress and deformation by a linear elastic analysis. This multi-scale framework based on inherent strain approach to predict the residual stress and deformation in LPBF process is clearly shown in Fig. 3. The element activation methods [69, 70] are used in both the detailed process and part-scale modeling to accelerate the numerical simulation. Their findings were very well matched with experimental results, and the method was shown to be more computationally practical than conventional thermo-mechanical simulations.

Following the proof of the inherent strain method’s suitability to the AM process, further studies were conducted in order to enhance this breakthrough. Bugatti and Semeraro [56] investigated the limitations of the inherent strain method (ISM) in the LPBF process both numerically and experimentally. They indicated that the macroscopic dimensional features had an influence on the inherent strain in their experiments, which implies that the basic geometry-independence assumption of inherent strain in the previous studies may be problematic. As a result, the ISM must be calibrated as the geometry becomes more complicated. Siewert et al. [71] delved deeper into the mechanical layer equivalent model by using the inherent

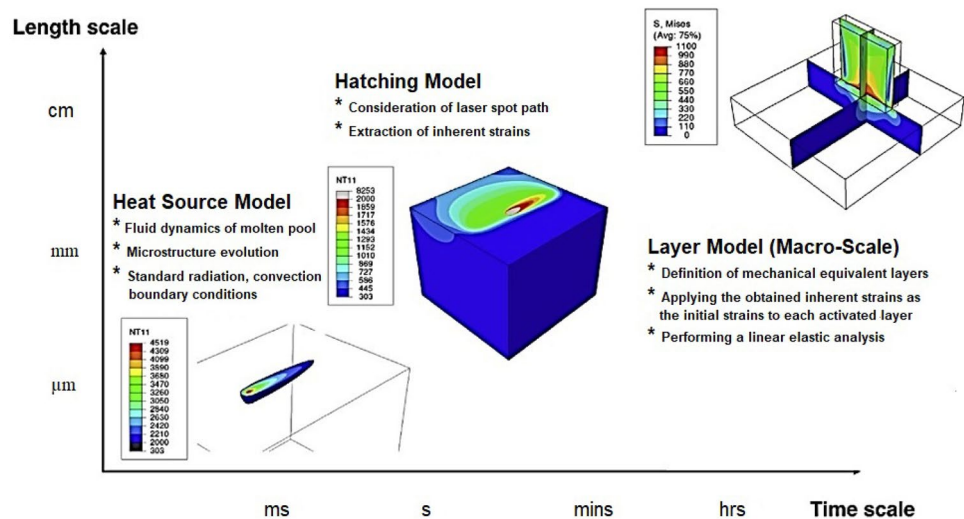
strains obtained from experimental calibration in two cantilever beams fabricated by LPBF. Their numerical model accurately predicted residual deformation based on experimental results. Ahmad et al. [72] indicated the consistency between the residual stress values estimated by inherent strain and contour methods. It was found that the formation of tensile and compressive residual stresses occurs near the surface (along the edges) and at the center area of samples, respectively. Furthermore, Setien et al. [73] presented an empirical methodology to determine inherent strains based on classical laminate theory (CLT) in composite laminates. They established a strong correlation between the sequential layer-wise LPBF process and the technology utilized to fabricate composite laminates. Considering the same effects of the hatching sequence and fiber orientation, the unique inherent strains that correspond to each layer are determined by iteratively optimizing the discrepancy between estimated residual distortions and experimental results of twin cantilever beams (Fig. 4). As a key finding of their research, the inter-layer inherent strains tend to be consistent when the laser scanning route turns regularly regardless of rotational angle. However, despite its good accuracy, the need for numerical optimization and the fabrication of a large number of samples restrict the use of this costly methodology in industry.

3 Modified inherent strain method (MISM)

3.1 Concept of MISM

The original inherent strain theory made the key assumption in the micro-scale simulation that the elastic strain is negligible in comparison to the plastic strain after the part is cooled down to room temperature. However, due to the

Fig. 3 Multi-scale framework using inherent strain approach to predict residual stress and deformation in LPBF [64]



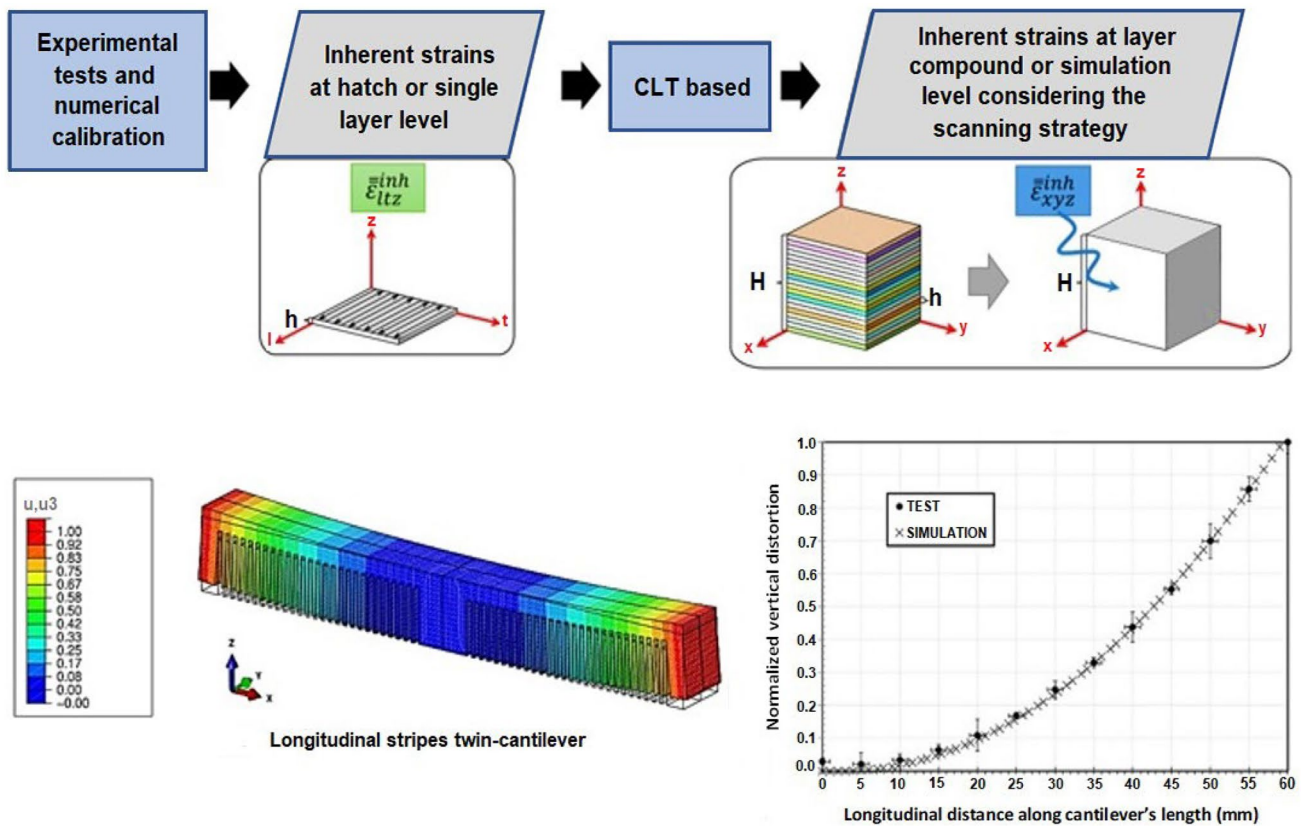


Fig. 4 Inherent strain determination strategy based on experimental tests for double cantilever beam [73]

difference between the physical phenomena of LPBF and the welding process resulting from the fast-moving heat source and multi-layer build model, this hypothesis cannot be employed in the LPBF process. Theoretically, throughout the LPBF, mechanical boundaries evolve with melting and solidification when additional layers are deposited, reaching a steady-state after printing subsequent layers. Thus, the elastic strain cannot be fully relieved when the part cools to ambient temperature [68]. The concept of the modified inherent strain method (MISM) was basically formulated by considering the contribution of two main factors during the process as follows:

$$\varepsilon^{In} = \varepsilon_{plastic}^I + (\varepsilon_{elastic}^I - \varepsilon_{elastic}^S) \quad (12)$$

where I and S represent the period of time belonging to the intermediate and steady-state conditions, respectively. In the modified version, the inherent strains taken from the meso-scale are implemented into the macro-scale as the constant coefficients of thermal expansion in x , y , and z directions, and a unit temperature increase is applied to each activated layer. Due to the much smaller value of the shear strains than the normal strains, the inherent shear strains are neglected in the multi-scale framework without sacrificing precision [68].

The mechanism of intermediate and steady states can be explained by the temperature and strain evolution of a bottom layer (first layer) in a 3-layer simulation through the MISM as illustrated in Fig. 5 [10]. Figure 5a represents the formation of compressive elastic and plastic strains at the early stage, as the material powder is sintered, which later transforms into tensile strain caused by further printed layers. The three sequential temperature peaks in Fig. 5b reflect the thermal history of the first deposited layer, with the second and third peaks resulting from succeeding layer depositions. According to Eq. (12), two significant sources are considered in the modified inherent strain theory: (1) the contribution from compressive plastic strain at the intermediate state and (2) the influence of thermal shrinkage coupled with the inter-layer effect. The accumulation of initially compressive strain in the intermediate state is due to a substantial drop in mechanical strength at an elevated temperature where the non-uniform thermal expansion, induced by a sharp temperature gradient in the melt pool area, is restrained by neighboring solidified metals. When the component is cooled to room temperature, the magnitude of compressive stress and strain is reduced, becoming tensile as a result of thermal contraction. Regarding the steady-state,

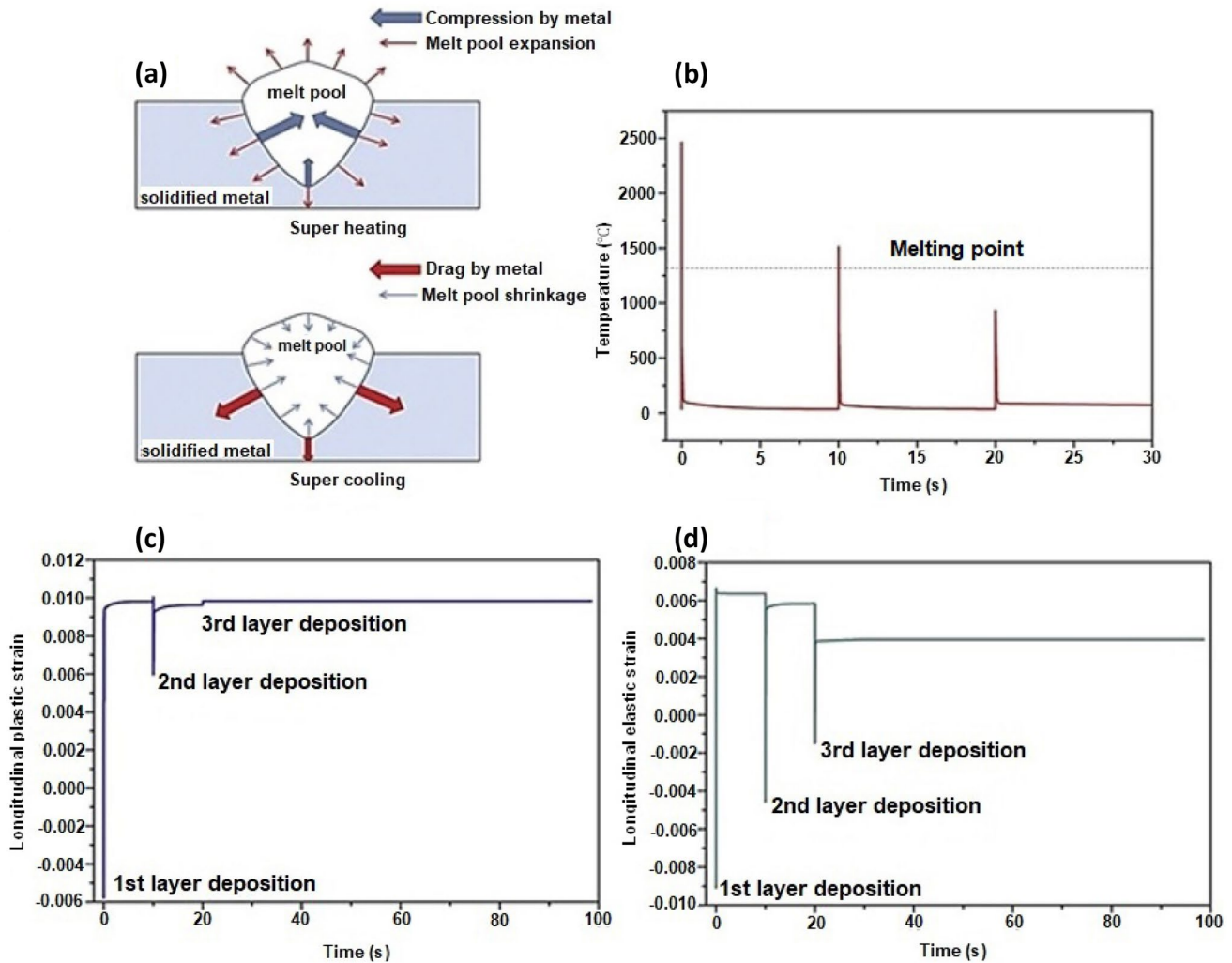


Fig. 5 a Mechanism of compressive and tensile strain; bottom layer b thermal history, c plastic strain, and d elastic strain evolution history [10]

Fig. 5c, d depict the significant relief of elastic strain by thermal shrinkage of surrounding solidified materials and previously deposited layers, demonstrating the small and profound impact of subsequent depositions on the plastic and elastic strain of the first layer, respectively. In the following sections, some groundbreaking research on MISM has been systematically reviewed.

3.2 Validation and layer lumping effect

Several recent studies have confirmed the validity and efficiency of the MISM when applied to the LPBF process. For instance, Chen et al. [10] estimated the deformation of a double cantilever beam and a complex canonical part by the MISM in LPBF process, which was in close agreement with experiments. They proved that the micro-scale modeling of 2-layer and 3-layer can nearly capture the same results due to the limited impact of the third deposition

on the strain evolution of the bottom layer. Furthermore, in another research study [74], they demonstrated that the residual deformation accuracy can be improved by more than 20% when using the MISM compared to the original inherent strain method in a double cantilever beam simulation. Moreover, according to the equivalent layer model in MISM, when a number of physical layers are lumped into one equivalent layer and a unit temperature rise is adopted to the equivalent layer in a load step, a particular number of lumped layers must be determined to accelerate the non-linear layer-by-layer simulation while ensuring accurate predictions. Their findings revealed that a thinner thickness of the activation layer (i.e., less layer lumping) would cause an underestimation of residual stress and deformation. The most plausible reason behind this phenomenon is that the tensile stress is generated in previous depositions due to the mechanical constraints induced by lower layers, and the thermal shrinkage of new deposited layers contributes to

the shrinkage of already deposited layers, resulting in an underestimation of tensile stress in lower layers due to the stress relief effect. Based on some simple numerical trials, the feasible layer activation thickness was identified as being between 0.4 and 0.6 mm for different cases [74]. However, the successive layer-by-layer simulation using 10–15 layer lumped was not still computationally practical for bulky parts. To tackle this issue, Liang et al. [75] proposed an enhanced layer lumping method (ELLM) in meso-scale modeling in which the material properties for the lumped super layers are modified to alleviate underestimation errors in the residual stress and deformation. The procedure has been shown in Fig. 6 in which the solid black line shows the stress–strain progression once one equivalent layer n is activated.

For the 2-super-layer situation, the n and $n + 1$ layers are activated concurrently, where the blue dashed line depicts the stress evolution associated with the bottom layer that attains to a lower magnitude in comparison with the activation of only one equivalent layer. The same scenario can be explained for the 3-super-layer case, as the lowest layer would behave like the red dashed line, and the $n + 1$ and $n + 2$ layers should behave as the blue dashed and solid black lines, respectively. Despite the simultaneous activation time for multiple equivalent layers in the lumped super layer method, various stress levels would emerge in different equivalent layers. As a result, specialized material constitutive models should be employed to modify the yield stress and inherent strains for distinct layers in ELLM to reduce overestimation errors. The accuracy, scalability, and robustness of ELLM were validated on a cantilever beam and a large complicated canonical part where the 4-layer ELLM case could reduce the simulation time by 70% [75]. Promoppatum and Uthaisangskul [64] explored the importance of optimizing the number of scanning paths to account for the influence of local preheating

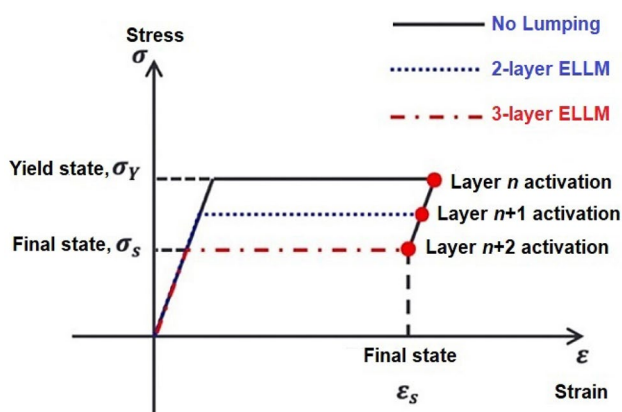


Fig. 6 The progress of residual stress and equivalent material models as a result of 2-layer and 3-layer lumping [75]

for the thermo-mechanical simulation of a single layer. In addition, concerning the relationship between the part's height and compressive stress accumulation, they asserted that the stress would transfer toward the center of the part as the height of the part becomes taller.

3.3 Simulation of the thin-walled lattice support structure by the MISM

Due to the high computational cost of performing a non-linear thermo-mechanical analysis of lattice support structures, Liang et al. [76] achieved pioneering research in adapting the MISM to these structures using the asymptotic homogenization technique. Following the MISM in previous studies, they obtained directional inherent strains through the meso-scale modeling of thin-walled as a representative volume element (RVE) given the periodicity of the macroscopic lattice support structures as shown in Fig. 7. An asymptotic homogenization approach [77] was then used to calculate RVE's equivalent thermal and mechanical parameters, including elastic modulus and inherent strains. After homogenizing the mechanical properties, the block made by the lattice support structure can be regarded as a solid continuum model in layer-wise simulation [76]. Not only did the postulated homogenization approach demonstrate good agreement with experimental measurements, but it also resulted in a tenfold increase in computational performance.

3.4 On the incorporation of scanning patterns into the MISM modeling

The laser scanning strategy is one of the crucial elements responsible for the anisotropy in the mechanical properties of parts manufactured by the LPBF process [78]. This issue confirms the longitudinal and transverse deviation in Young's modulus and yield strength of many LPBF components with respect to the laser moving direction. On the

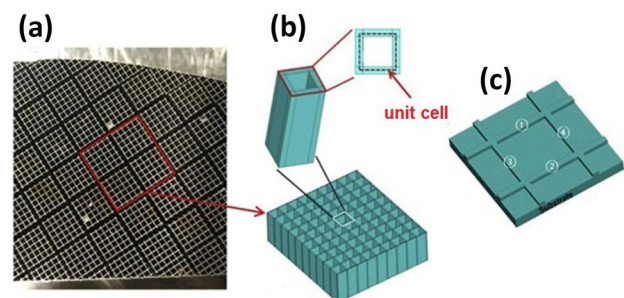


Fig. 7 **a** The thin-walled lattice support structures in LPBF; **b** the representative unit cell (red dashed square); **c** the representative volume for small-scale modeling [76]

other hand, the layer-by-layer fashion rotational laser scanning method has less impact on the mechanical properties compared to the unidirectional scanning approach partially due to the high dependency of microstructures on temperature gradients caused by the laser moving direction [78]. Concerning the impact of anisotropy on residual deformation, Liang et al. [79] investigated the effects of various laser scanning strategies included in MISM to accurately predict the residual deformation of the LPBF components. Despite the parallel line (PL) laser scanning strategy, where the directional material properties like inherent strains and elastic modulus can be implemented in a single local elemental coordinate system (LECS) toward the laser moving direction, in the rotational line (RL) laser scanning strategy, the LECS should be separately assigned to different layers according to the laser moving direction. To satisfy both accuracy and efficiency in the finite element analysis of a large model, the asymptotic homogenization method [77] was employed to extract the equivalent elastic modulus and the correct form of the modified inherent strain vector for the RL laser scanning pattern. Technically, the homogenized inherent strain vector (HISV) can be computed by assigning the directional inherent strain vector attained from small-scale modeling to a number of lumped real layers as the coefficients of thermal expansion in accordance with the laser scanning direction for each thin layer. The number of merged layers is considered a representative volume element (RVE) as the smallest repetitive volume. The height of this RVE depends on the regularity of the rotational laser scanning routes in a part. As an example, Fig. 8 illustrates a 3-layer RVE for the 60°-RL laser scanning pattern with a

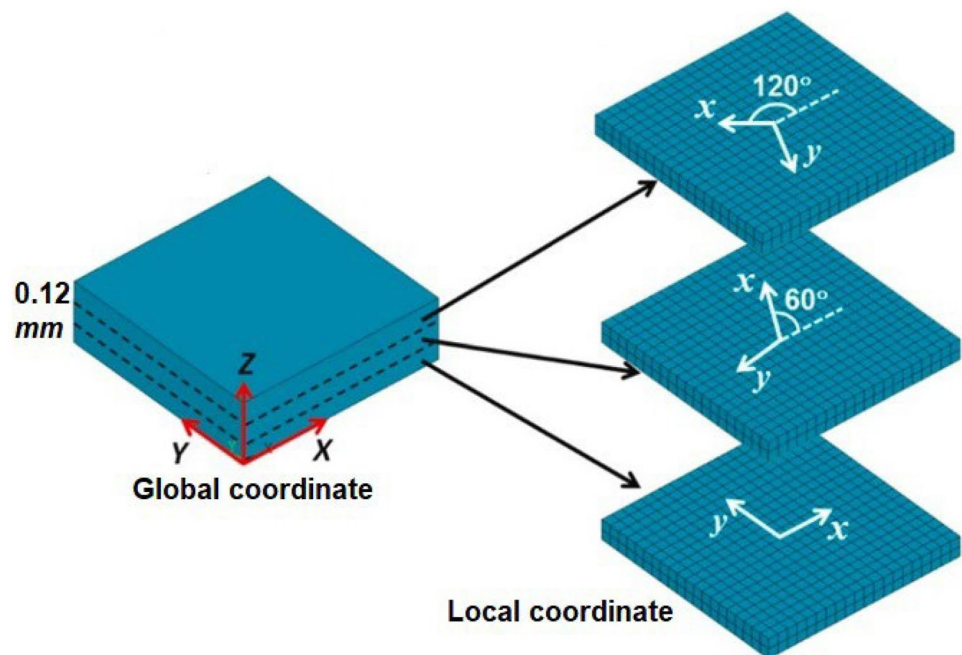
layer thickness of 40 μm , which shows that at least 3 layers are necessary to achieve a 180° rotation of the laser scanning line relative to the initial position of the laser moving vector direction. Finally, the homogenized elastic modulus and HISV are used in a layer-by-layer fashion irrespective of the laser scanning strategies to measure the residual deformation in an efficient way [79].

The incorporation of scanning strategies into MISM has been validated by the experimental data, ensuring excellent accuracy of the proposed workflow. Besides the capability of this comprehensive method to be used in many cases involving RL laser scanning strategies, the development of this methodology with the integration of anisotropic plastic yielding law is a potential future work suggested by the authors.

3.5 Improved modified inherent strain method

Although the MISM demonstrated its ability to accurately compute the residual deformation in LPBF parts, its accuracy in the residual stress prediction was not still validated. To do so, Dong et al. [80] conducted detailed investigation to evaluate the capability of the existing MISM to fairly estimate residual stress distribution without affecting the prediction of residual deformation. In the first step, a 3-layer single-walled structure was modeled to compare the residual stress accumulation between the detailed simulation results and the existing MISM. To capture a precise broad range of temperature-dependent material properties, they applied a cut-off temperature, recommended by Lindgren [81], beyond which the material properties remain unchanged.

Fig. 8 The 3-layer RVE model in the local and global coordinate systems for a 60°-RL laser scanning pattern [79]



After performing the numerical analyses, despite the good agreement in the maximum residual deformation predicted by the two processes, the obtained residual von Mises stress was overestimated by the MISM, which was much higher than the detailed simulation (close to the yield strength). Therefore, the existing MISM approach failed to measure residual stress precisely. The first attempt was to identify the potential source of the error. Due to the valid residual deformation results, they concluded that the inherent strain values measured in the meso-scale stage are trustworthy and an inaccurate relative percentage of elastic and plastic strains in total strains may give rise to an overestimation in predicted residual stress level. They reported that the use of constant ambient temperature material properties in macro-scale modeling may be a possible source of inaccuracy [80]. As mentioned in Sect. 3.1, over the span of two phases, namely, intermediate and steady state, the local and global temperature gradients induce strains, respectively. Thus, in the macro-scale modeling of MISM, in order to reach an accurate proportion between the final elastic and plastic strains, both the effects of localized and global thermal gradients must be included, which implies that using just material properties at ambient temperature cannot satisfy this condition. Based on this hypothesis, a new implementation procedure for the MIS-based simulation was proposed in which two consecutive static analyses are performed using the material properties at the intermediate and steady-state temperatures, respectively, while the inherent strains are kept constant in both steps [80]. Figure 9 provides a detailed description of both the existing and the new MISM. As a demonstration of the new procedure's validity with respect to the detailed simulation results, the von Mises stress field for a 3-layer thin-walled model is represented in Fig. 10 where the new MISM offers better residual stress prediction compared to the existing one. Furthermore, to assess the viability of the new MISM experimentally, the L-bracket and canonical parts were printed, and the good agreement between numerical and experimental results indicated the sound performance of the new implementation [80].

3.6 Optimization based on the ISM

In the last couple of years, innovative optimization techniques based on the inherent strain method have been developed to identify the optimum design parameters with the goal of lowering the detrimental residual stresses and volume of the support structure. As the most patently examples, Cheng and To [82] proposed a multi-objective optimization methodology to automatically define the optimal build orientation for complicated parts. In their modeling, the stress distribution in the support structure was calculated by the voxel-based fictitious domain (i.e. finite cell method)

rather than the conformal mesh to avoid time-consuming mesh generation during the optimization process. It was found that not only does the suggested method mitigate the impact of residual stress in the build part, but it also secures the design manufacturability while diminishing the material consumption for the support structure. In another study, Zhang et al. [83] executed the topology optimization and inherent strain method for the support structure by considering the gravity load in the objective function to reduce the before and after-cutting deflections in printed cantilevers. Their experimental and numerical (ISM) findings revealed that the optimized supports may reduce component deflection and material consumption by more than 60% and 50%, respectively, compared to the default support structure. Examining the feasibility of the part-scale topology optimization for continuum and lattice support structure design via the inherent strain method was also carried out by other researchers [83–87]. Besides confirming previous findings on advantage of optimized support structure on mitigation of residual stress and part deformation, it was also observed that stress-induced cracking would no longer appear in the parts with optimized support structure.

As previously mentioned, according to the anisotropic nature of the local deformation caused by the moving heat source in the LPBF process, the scanning route may dramatically alter residual stress inside a component. Scanning path optimization has thus been proved to be an efficient solution in the reduction of residual stress and deformation. For instance, Chen et al. [88] proposed a novel method to perform continuous layer-by-layer scanning path optimization using the inherent strain method. A numerical strategy, namely, adaptive level set adjustment (ALSA), was employed to ameliorate the detrimental effect of disregarding a portion of the sensitivity result. Typically, the level set technique is a mathematical framework for assessing and monitoring implicit moving interfaces [89]. It was observed that the zero-level set contour continues to shrink, until it comprises a very small portion of the design domain, causing the optimization problem fails to converge. In this situation, the ALSA technique tries to keep the zero-level set contour inside the design domain during the process optimization, achieving a good convergence for both compliance and stress minimization problems. This scalable approach demonstrated its ability to be used for parts with more complicated geometrical features, extending to integrating both topology and laser scanning path optimization simultaneously [88]. The island scanning pattern optimization method was another study conducted by Chen et al. [90] to reduce part deformation. Considering the scanning orientation-dependent inherent strain vector associated with each island in a given geometry as a design variable, finite element analysis was used to determine the optimal scanning direction

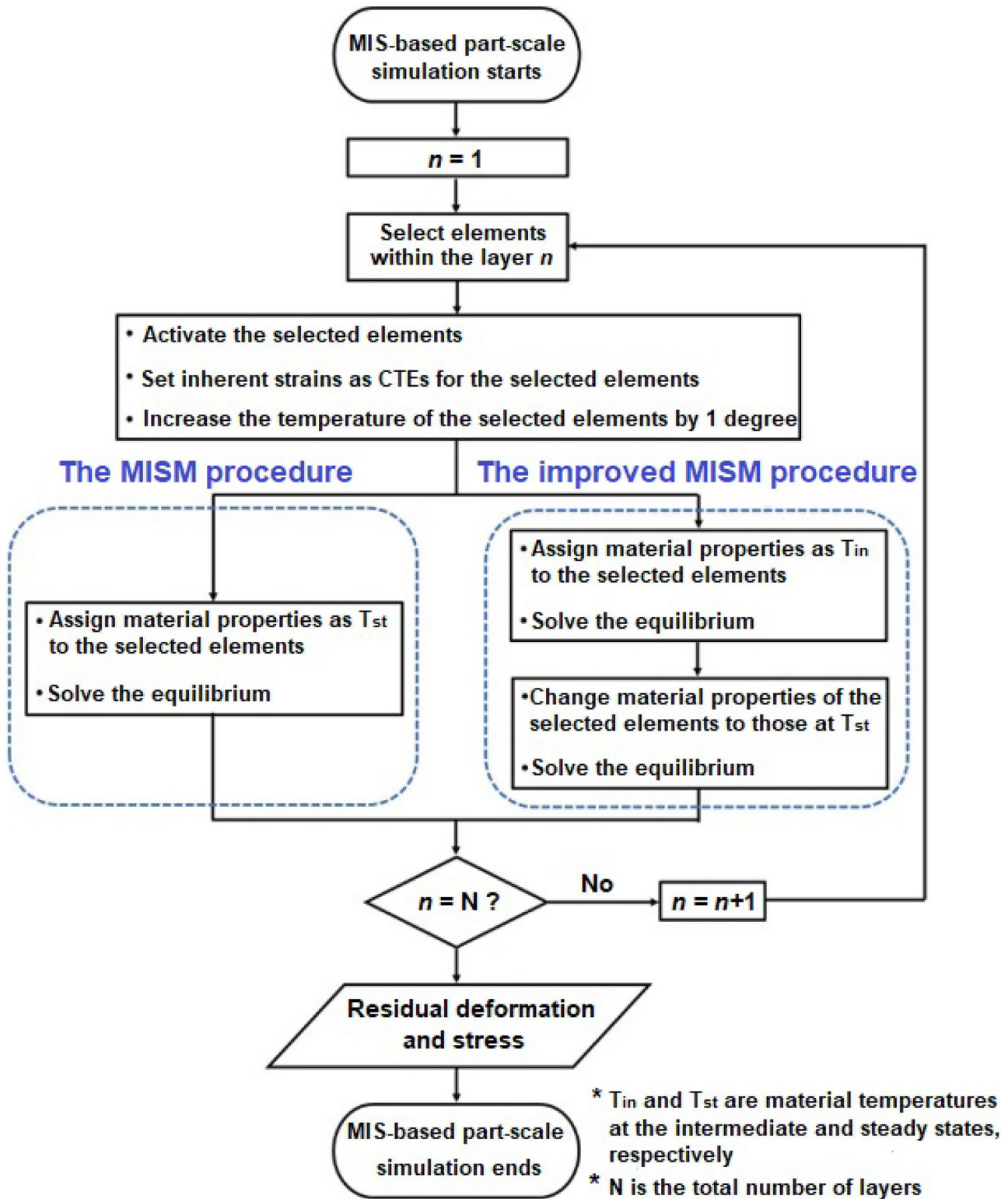


Fig. 9 Comparison of the existing and new procedures for MIS-based part-scale simulation [80]

for each island through an iterative optimization algorithm. The feasibility and effectiveness of the suggested method were experimentally validated on a block structure and a

connecting rod. A considerable reduction in residual deformation of the two parts was achieved by over 50% compared with the initial scanning pattern.

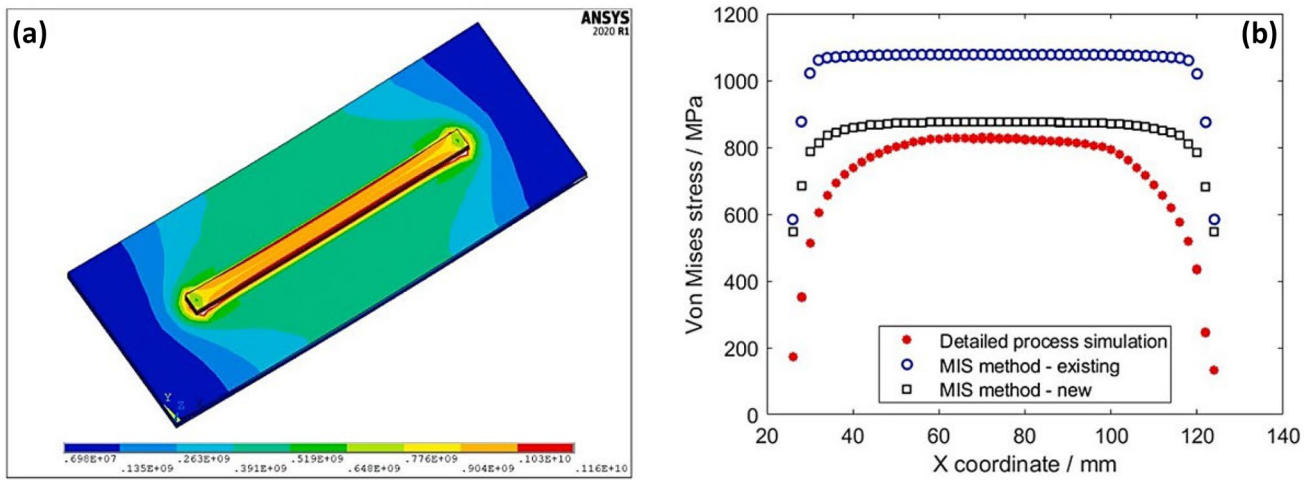


Fig. 10 **a** Von Mises stress field; **b** comparison of the von Mises stress along the top centerline in different simulations [80]

The principle for hatch pattern optimization was explored by Li and Anand [91] via developing an innovative neural network-based model, capable of predicting inherent strains for any given hatch pattern used in the part build. They trained a feedforward propagation neural network model with inherent strain values obtained from an initial hatch pattern and validated with the inherent strain data attained from subsequent hatch pattern using the micro-scale detailed simulation. The neural network examines the correlation between the hatch angles of various layers to determine the total inherent strain. Figure 11 represents the overall methodology of the suggested approach step by step. It was shown that trained neural network could estimate the inherent strain of any randomly hatch pattern with less than 8% inaccuracy.

4 Practical implications of the research

This section highlights some of the practical implications of this research derived from two components reviewed previously in this paper. In the optimization-based problems, the numerical method may require hundreds of iterations to converge, and each iteration demands a part-scale residual stress calculation. Using a high-fidelity ISM-based numerical model in which the LPBF process is replicated based on the actual process parameters can be the most accurate and efficient way to predict the residual stress and distortion. The salient feature of the inherent strain approach is that it replaces the computationally costly detailed thermo-mechanical simulation with a pure mechanical analysis. This enables physics-based iterative optimization to systematically

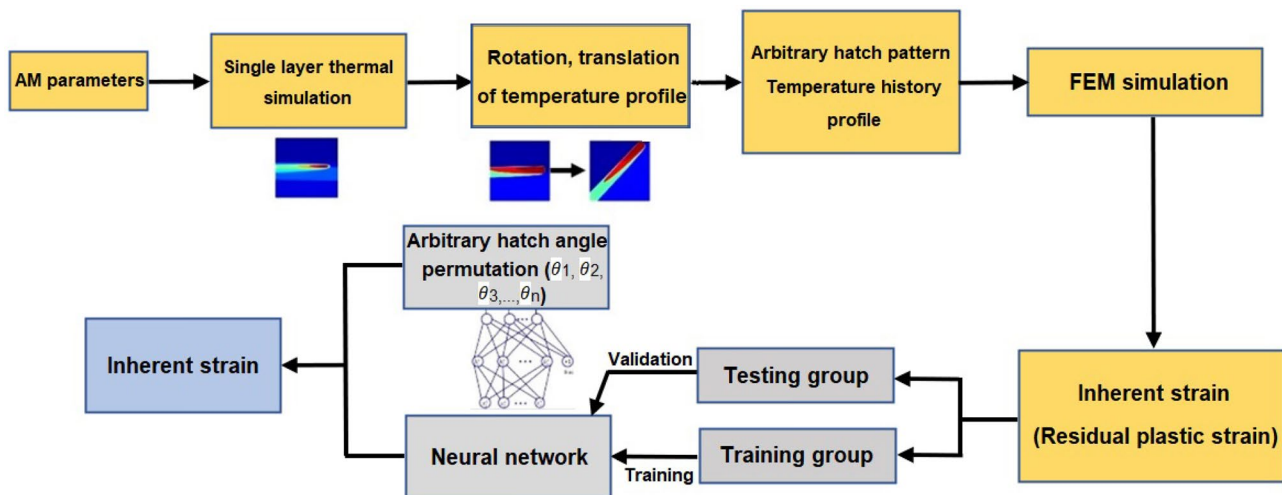


Fig. 11 Flowchart of the proposed neural network-based method to predict inherent strain [91]

remove residual stress-induced build failure [82]. Moreover, when lattice support structures are employed in build of the parts with overhanging structure, the detailed simulation of the LPBF process becomes more complicated due to the difficulty in mesh generation and the implementation of the exact laser scanning strategy and process parameters. Using the ISM can facilitate to efficiently predict the residual deformation of those AM components with open-cell lattice structure in terms of topological features and physical printing manners. Therefore, due to the wide range of industrial applications for the parts fabricated by the LPBF, the implementation of high-fidelity and efficient numerical methods such as the ISM, not only the computational cost is significantly reduced, but in terms of sustainability, it may establish an industry that is smarter and more efficient (less material waste and faster supply chains).

5 Conclusions and future directions

In this paper, a detailed review is performed on the development of the inherent strain method as an efficient technique compared to the conventional thermo-mechanical simulation in LPBF additive manufacturing process. A brief discussion was first presented on the coupled thermo-mechanical simulations, including their energy, temperature displacement, and governing mechanical formulations. Due to the inaccurate residual stress and deformation predictions resulting from the original inherent strain method, the proposed modified version demonstrated its ability to provide a more precise analysis of inherent strains considering the contribution of residual strain in the intermediate and final steady states of the depositions. Moreover, the application of the MISM to the thin-walled lattice support structure by using the asymptotic homogenization method was reviewed demonstrating its capability to dramatically enhance the computational performance. It was shown that the improved MISM can predict the residual stress in excellent agreement with experimental results by taking into account the effect of both local and global thermal gradients on the temperature-dependent material properties.

Thus far, much research has been conducted using the inherent strain method to evaluate the influence of some contributing factors, such as layer lumping effect, scanning strategy, and process optimization on the formation of residual stress and deformation. However, there are still some important parameters like strain and rate of hardening in the plastic yielding law or the influence of phase transformation in the microstructure evolution [92] that can be a potential source of error since they were overlooked in the majority of the recent inherent strain-based investigations. Therefore, it is expected that future research attempts will be directed toward determining the effect of these characteristics on the prediction made by

the MIS approach. On the other hand, incorporating machine learning methods such as neural networks to connect a large number of process parameters to the associated inherent strains is a captivating outlook by which a large database can be used to train the neural networks with the aim of building a relationship between undeformed and deformed geometry, compensating for the distortion in the metal parts [93]. Moreover, formal design optimization formulation to identify optimal process and geometrical parameters in the LPBF to minimize the part distortion due to induced residual stresses has not been investigated. Combination of high-fidelity-validated finite element model and deep learning artificial intelligence algorithm as a growing trend may provide unique opportunity to develop computationally efficient reduced order models to be practically used in optimization formulation.

Author contribution All authors contributed to the study conception and design. Material preparation, data collection, and analysis were performed by Hossein Mohammadtaheri. The first draft of the manuscript was written by Hossein Mohammadtaheri, and all authors commented on previous versions of the manuscript. All authors read and approved the final manuscript.

Funding This work was conducted as part of a project supported by the National Research Council's METALTec Industrial Research Group, the National Research Council's National Program Office (NPO), and the Metal Transformation Research and Innovation Consortium (CRITM) as well with grant number AM-113-3.

Availability of data and material Not applicable.

Code availability Not applicable.

Declarations

Ethics approval Not applicable.

Consent to participate Not applicable.

Consent for publication Not applicable.

Conflict of interest The authors declare no competing interests.

References

1. Pragana JPM, Sampaio RFV, Bragança IMF, Silva CMA, Martins PAF (2021) Hybrid metal additive manufacturing: a state-of-the-art review. *Adv Ind Manuf Eng* 2:100032
2. Frazier WE (2014) Metal additive manufacturing: a review. *J Mater Eng Perform* 23:1917–1928
3. Teng C, Gong H, Szabo A, Dilip JJS, Ashby K, Zhang S, Patil N, Pal D, Stucker B (2017) Simulating melt pool shape and lack of fusion porosity for selective laser melting of cobalt chromium components. *J Manuf Sci Eng Trans ASME* 139:1–11
4. Buchbinder D, Meiners W, Pirch N, Wissenbach K, Schrage J (2014) Investigation on reducing distortion by preheating during manufacture of aluminum components using selective laser melting. *J Laser Appl* 26:012004

5. Kempen K, Vrancken B, Buls S, Thijs L, Van Humbeeck J, Kruth JP (2014) Selective laser melting of crack-free high density M2 high speed steel parts by baseplate preheating. *J Manuf Sci Eng Trans ASME* 136:1–7
6. Li C, Fu CH, Guo YB, Fang FZ (2015) A multiscale modeling approach for fast prediction of part distortion in selective laser melting. *J Mater Process Technol* 229:703–712
7. Stavropoulos P, Foteinopoulos P, Papacharalampopoulos A, Tsoukantas G (2019) Warping in SLM additive manufacturing processes: estimation through thermo-mechanical analysis. *Int J Adv Manuf Technol* 104:1571–1580
8. Bauereiß A, Scharowsky T, Körner C (2014) Defect generation and propagation mechanism during additive manufacturing by selective beam melting. *J Mater Process Technol* 214:2522–2528
9. Gouge M, Michaleris P, Denlinger E, Irwin J (2018) The finite element method for the thermo-mechanical modeling of additive manufacturing processes, 1st ed. *Thermo-Mechanical Model Addit Manuf*. <https://doi.org/10.1016/B978-0-12-811820-7.00003-3>
10. Chen Q, Liang X, Hayduke D, Liu J, Cheng L, Oskin J, Whitmore R, To AC (2019) An inherent strain based multiscale modeling framework for simulating part-scale residual deformation for direct metal laser sintering. *Addit Manuf* 28:406–418
11. Yang Q, Zhang P, Cheng L, Min Z, Chyu M, To AC (2016) Finite element modeling and validation of thermomechanical behavior of Ti-6Al-4V in directed energy deposition additive manufacturing. *Addit Manuf* 12:169–177
12. Dunbar AJ, Denlinger ER, Gouge MF, Simpson TW, Michaleris P (2017) Comparisons of laser powder bed fusion additive manufacturing builds through experimental in situ distortion and temperature measurements. *Addit Manuf* 15:57–65
13. Mercelis P, Kruth JP (2006) Residual stresses in selective laser sintering and selective laser melting. *Rapid Prototyp J* 12:254–265
14. An K, Yuan L, Dial L, Spinelli I, Stoica AD, Gao Y (2017) Neutron residual stress measurement and numerical modeling in a curved thin-walled structure by laser powder bed fusion additive manufacturing. *Mater Des* 135:122–132
15. Levkulich NC, Semiatin SL, Gockel JE, Middendorf JR, DeWald AT, Klingbeil NW (2019) The effect of process parameters on residual stress evolution and distortion in the laser powder bed fusion of Ti-6Al-4V. *Addit Manuf* 28:475–484
16. Wu AS, Brown DW, Kumar M, Gallegos GF, King WE (2014) An experimental investigation into additive manufacturing-induced residual stresses in 316L stainless steel. *Metall Mater Trans A Phys Metall Mater Sci* 45:6260–6270
17. Sochalski-Kolbus LM, Payzant EA, Cornwell PA, Watkins TR, Babu SS, Dehoff RR, Lorenz M, Ovchinnikova O, Duty C (2015) Comparison of residual stresses in Inconel 718 simple parts made by electron beam melting and direct laser metal sintering. *Metall Mater Trans A Phys Metall Mater Sci* 46:1419–1432
18. Keshavarzkermani A, Marzbanrad E, Esmaeilizadeh R, Mahmoodkhani Y, Ali U, Enrique PD, Zhou NY, Bonakdar A, Toyserkani E (2019) An investigation into the effect of process parameters on melt pool geometry, cell spacing, and grain refinement during laser powder bed fusion. *Opt Laser Technol* 116:83–91
19. Kumar P, Farah J, Akram J, Teng C, Ginn J, Misra M (2019) Influence of laser processing parameters on porosity in Inconel 718 during additive manufacturing. *Mater Lett* 103:1497–1507
20. Yeung H, Lane B (2020) A residual heat compensation based scan strategy for powder bed fusion additive manufacturing. *Manuf Lett* 25:56–59
21. Ghayoor M, Lee K, He Y, Chang CH, Paul BK, Pasebani S (2020) Selective laser melting of 304L stainless steel: role of volumetric energy density on the microstructure, texture and mechanical properties. *Addit Manuf*. <https://doi.org/10.1016/j.addma.2019.101011>
22. Kantzos C, Pauza J, Cunningham R, Narra SP, Beuth J, Rollett A (2019) An investigation of process parameter modifications on additively manufactured Inconel 718 parts. *J Mater Eng Perform* 28:620–626
23. Young ZA, Guo Q, Parab ND, Zhao C, Qu M, Escano LI, Fezzaa K, Everhart W, Sun T, Chen L (2020) Types of spatter and their features and formation mechanisms in laser powder bed fusion additive manufacturing process. *Addit Manuf* 36:101438
24. Gockel J, Sheridan L, Koerper B, Whip B (2019) The influence of additive manufacturing processing parameters on surface roughness and fatigue life. *Int J Fatigue* 124:380–388
25. Nayak SK, Mishra SK, Jinoop AN, Paul CP, Bindra KS (2020) Experimental studies on laser additive manufacturing of Inconel-625 structures using powder bed fusion at 100 µm layer thickness. *J Mater Eng Perform* 29:7636–7647
26. Vastola G, Zhang G, Pei QX, Zhang YW (2016) Controlling of residual stress in additive manufacturing of Ti6Al4V by finite element modeling. *Addit Manuf* 12:231–239
27. Soundararajan B, Sofia D, Barletta D, Poletto M (2021) Review on modeling techniques for powder bed fusion processes based on physical principles. *Addit Manuf* 47:102336
28. Karayagiz K, Elwany A, Tapia G, Franco B, Johnson L, Ma J, Karaman I, Arróyave R (2019) Numerical and experimental analysis of heat distribution in the laser powder bed fusion of Ti-6Al-4V. *IJSE Trans* 51:136–152
29. Wessels H, Weissenfels C, Wriggers P (2018) Metal particle fusion analysis for additive manufacturing using the stabilized optimal transportation meshfree method. *Comput Methods Appl Mech Eng* 339:91–114
30. Denlinger ER, Heigel JC, Michaleris P, Palmer TA (2015) Effect of inter-layer dwell time on distortion and residual stress in additive manufacturing of titanium and nickel alloys. *J Mater Process Technol* 215:123–131
31. Lindgren LE, Lundbäck A, Fisk M, Pederson R, Andersson J (2016) Simulation of additive manufacturing using coupled constitutive and microstructure models. *Addit Manuf* 12:144–158
32. Chen C, Xiao Z, Zhu H, Zeng X (2020) Deformation and control method of thin-walled part during laser powder bed fusion of Ti-6Al-4V alloy. *Int J Adv Manuf Technol* 110:3467–3478
33. Denlinger ER, Gouge M, Irwin J, Michaleris P (2017) Thermomechanical model development and in situ experimental validation of the laser powder-bed fusion process. *Addit Manuf* 16:73–80
34. Mukherjee T, Zhang W, DebRoy T (2017) An improved prediction of residual stresses and distortion in additive manufacturing. *Comput Mater Sci* 126:360–372
35. Cheng B, Shrestha S, Chou K (2016) Stress and deformation evaluations of scanning strategy effect in selective laser melting. *Addit Manuf* 12:240–251
36. Hussein A, Hao L, Yan C, Everson R (2013) Finite element simulation of the temperature and stress fields in single layers built without-support in selective laser melting. *Mater Des* 52:638–647
37. Chiumenti M, Neiva E, Salsi E, Cervera M, Badia S, Moya J, Chen Z, Lee C, Davies C (2017) Numerical modelling and experimental validation in selective laser melting. *Addit Manuf* 18:171–185
38. Zaeh MF, Branner G (2010) Investigations on residual stresses and deformations in selective laser melting. *Prod Eng* 4:35–45
39. Afazov S, Denmark WAD, Lazaro Toralles B, Holloway A, Yaghi A (2017) Distortion prediction and compensation in selective laser melting. *Addit Manuf* 17:15–22
40. Ganeriwala RK, Strantz M, King WE, Clausen B, Phan TQ, Levine LE, Brown DW, Hodge NE (2019) Evaluation of a thermomechanical model for prediction of residual stress during laser powder bed fusion of Ti-6Al-4V. *Addit Manuf* 27:489–502

41. Li C, Liu ZY, Fang XY, Guo YB (2018) On the simulation scalability of predicting residual stress and distortion in selective laser melting. *J Manuf Sci Eng Trans ASME*. <https://doi.org/10.1115/1.4038893>
42. Patil N, Pal D, Rafi HK, Zeng K, Moreland A, Hicks A, Beeler D, Stucker B (2015) A generalized feed forward dynamic adaptive mesh refinement and derefinement finite element framework for metal laser sintering - part I: Formulation and algorithm development. *J Manuf Sci Eng Trans ASME*. <https://doi.org/10.1115/1.4030059>
43. Pal D, Patil N, Kutty KH, Zeng K, Moreland A, Hicks A, Beeler D, Stucker B (2016) A generalized feed-forward dynamic adaptive mesh refinement and derefinement finite-element framework for metal laser sintering-part II: nonlinear thermal simulations and validations. *J Manuf Sci Eng Trans ASME* 138:1–10
44. Denlinger ER, Irwin J, Michaleris P (2014) Thermomechanical modeling of additive manufacturing large parts. *J Manuf Sci Eng Trans ASME*. <https://doi.org/10.1115/1.4028669>
45. Gouge M, Denlinger E, Irwin J, Li C, Michaleris P (2019) Experimental validation of thermo-mechanical part-scale modeling for laser powder bed fusion processes. *Addit Manuf*. <https://doi.org/10.1016/j.addma.2019.06.022>
46. Li C, Denlinger ER, Gouge MF, Irwin JE, Michaleris P (2019) Numerical verification of an Octree mesh coarsening strategy for simulating additive manufacturing processes. *Addit Manuf*. <https://doi.org/10.1016/j.addma.2019.100903>
47. Hajjalizadeh F, Ince A (2019) Finite element-based numerical modeling framework for additive manufacturing process. *Mater Des Process Commun* 1:1–7
48. Papadakis L, Loizou A, Risse J, Schrage J (2014) Numerical computation of component shape distortion manufactured by Selective Laser Melting. *Procedia CIRP* 18:90–95
49. Alvarez P, Ecenarro J, Setien I, Sebastian MS, Echeverria A, Eciolaza L (2016) Computationally efficient distortion prediction in powder bed fusion additive manufacturing. *Int J Eng Res Sci* 39–46
50. Ueda Y, Yuan MG (1993) Prediction of residual stresses in butt welded plates using inherent strains. *J Eng Mater Technol Trans ASME* 115:417–423
51. Ueda Y, Fukuda KTM (1979) New measuring method of three-dimensional residual stresses based on theory of inherent strain (welding mechanics, strength & design). *Trans JWRI* 8(2):249–256
52. Zhang L, Michaleris P, Marugabandhu P (2007) Evaluation of applied plastic strain methods for welding distortion prediction. *J Manuf Sci Eng Trans ASME* 129:1000–1010
53. Michaleris P, Zhang L, Bhide SR, Marugabandhu P (2006) Evaluation of 2D, 3D and applied plastic strain methods for predicting buckling welding distortion and residual stress. *Sci Technol Weld Join* 11:707–716
54. Denlinger ER (2018) Residual stress and distortion modeling of electron beam direct manufacturing Ti-6Al-4V, 1st ed. *Thermo-Mechanical Model Addit Manuf*. <https://doi.org/10.1016/B978-0-12-811820-7.00011-2>
55. Keller N, Ploshikhin V (2014) New method for fast predictions of residual stress and distortion of AM parts. *Solid Free Fabr Symp* 1:1229–1237
56. Bugatti M, Semeraro Q (2018) Limitations of the inherent strain method in simulating powder bed fusion processes. *Addit Manuf* 23:329–346
57. Yang Y, Allen M, London T, Oancea V (2019) Residual strain predictions for a powder bed fusion Inconel 625 single cantilever part. *Integr Mater Manuf Innov* 8:294–304
58. Afazov S, Rahman H, Serjouei A (2021) Investigation of the right first-time distortion compensation approach in laser powder bed fusion of a thin manifold structure made of Inconel 718. *J Manuf Process* 69:621–629
59. Mayer T, Brändle G, Schönenberger A, Eberlein R (2020) Simulation and validation of residual deformations in additive manufacturing of metal parts. *Heliyon*. <https://doi.org/10.1016/j.heliyon.2020.e03987>
60. Hajjalizadeh F, Ince A (2020) Short review on modeling approaches for metal additive manufacturing process. *Mater Des Process Commun* 2:1–7
61. Luo Z, Zhao Y (2018) A survey of finite element analysis of temperature and thermal stress fields in powder bed fusion additive manufacturing. *Addit Manuf* 21:318–332
62. Hetnarski RB, Eslami MR (2009) Thermal stresses - Advanced theory and applications. *Solid Mech its Appl*. https://doi.org/10.1007/978-1-4020-9247-3_1
63. Hare CH (1996) Thermal stresses. *J Prot Coatings Linings*. <https://doi.org/10.1201/9780203735831>
64. Promopattum P, Uthaisangskuk V (2021) Part scale estimation of residual stress development in laser powder bed fusion additive manufacturing of Inconel 718. *Finite Elem Anal Des*. <https://doi.org/10.1016/j.finel.2021.103528>
65. Marcotte J-P, Kabanemi K, Molavi-Zarandi M, Ilinca F, Cagnone J-S (2021) Development of a thermomechanical model for prediction of residual stress during laser powder-bed fusion: Evaluation of inherent strain approach. 14th World Congress in Computational Mechanics (WCCM). <https://doi.org/10.23967/wccm-eccomas.2020.120>
66. Kabir IR, Yin D, Tamanna N, Naher S (2018) Thermomechanical modelling of laser surface glazing for H13 tool steel. *Appl Phys A Mater Sci Process* 124:1–9
67. Johnson GR, Cook WH (1983) A computational constitutive model and data for metals subjected to large strain, high strain rates and high pressures. *Seventh Int Symp Ballist* 541–547
68. Liang X, Cheng L, Chen Q, Yang Q, To AC (2018) A modified method for estimating inherent strains from detailed process simulation for fast residual distortion prediction of single-walled structures fabricated by directed energy deposition. *Addit Manuf* 23:471–486
69. Lindgren LE, Runnemalm H, Näsström MO (1999) Simulation of multipass welding of a thick plate. *Int J Numer Methods Eng* 44:1301–1316
70. Michaleris P (2014) Modeling metal deposition in heat transfer analyses of additive manufacturing processes. *Finite Elem Anal Des* 86:51–60
71. Siewert M, Neugebauer F, Epp J, Ploshikhin V (2019) Validation of mechanical layer equivalent method for simulation of residual stresses in additive manufactured components. *Comput Math with Appl* 78:2407–2416
72. Ahmad B, van der Veen SO, Fitzpatrick ME, Guo H (2018) Residual stress evaluation in selective-laser-melting additively manufactured titanium (Ti-6Al-4V) and inconel 718 using the contour method and numerical simulation. *Addit Manuf* 22:571–582
73. Setien I, Chiumenti M, van der Veen S, San Sebastian M, Garcíandía F, Echeverría A (2019) Empirical methodology to determine inherent strains in additive manufacturing. *Comput Math with Appl* 78:2282–2295
74. Liang X, Chen Q, Cheng L, Hayduke D, To AC (2019) Modified inherent strain method for efficient prediction of residual deformation in direct metal laser sintered components. *Comput Mech* 64:1719–1733
75. Liang X, Hayduke D, To AC (2021) An enhanced layer lumping method for accelerating simulation of metal components produced by laser powder bed fusion. *Addit Manuf* 39:101881
76. Liang X, Dong W, Hinnebusch S, Chen Q, Tran HT, Lemon J, Cheng L, Zhou Z, Hayduke D, To AC (2020) Inherent strain

- homogenization for fast residual deformation simulation of thin-walled lattice support structures built by laser powder bed fusion additive manufacturing. *Addit Manuf*. <https://doi.org/10.1016/j.addma.2020.101091>
77. Bensoussan A, Lions J-L, Papanicolaou G (2011) Asymptotic analysis for periodic structures. American Mathematical Society, vol 374. AMS Chelsea Publishing
 78. Robinson JH, Ashton IRT, Jones E, Fox P, Sutcliffe C (2019) The effect of hatch angle rotation on parts manufactured using selective laser melting. *Rapid Prototyp J* 25:289–298
 79. Liang X, Dong W, Chen Q, To AC (2021) On incorporating scanning strategy effects into the modified inherent strain modeling framework for laser powder bed fusion. *Addit Manuf* 37:101648
 80. Dong W, Liang X, Chen Q, Hinnebusch S, Zhou Z, To AC (2021) A new procedure for implementing the modified inherent strain method with improved accuracy in predicting both residual stress and deformation for laser powder bed fusion. *Addit Manuf* 47:102345
 81. Lindgren L-E (2014) Computational welding mechanics. Woodhead Publishing, Elsevier, ISBN: 9781845693558
 82. Cheng L, To A (2019) Part-scale build orientation optimization for minimizing residual stress and support volume for metal additive manufacturing: theory and experimental validation. *CAD Comput Aided Des* 113:1–23
 83. Zhang ZD, Ibhadode O, Ali U, Dibia CF, Rahnama P, Bonakdar A, Toyserkani E (2020) Topology optimization parallel-computing framework based on the inherent strain method for support structure design in laser powder-bed fusion additive manufacturing. *Int J Mech Mater Des* 16:897–923
 84. Cheng L, Liang X, Bai J, Chen Q, Lemon J, To A (2019) On utilizing topology optimization to design support structure to prevent residual stress induced build failure in laser powder bed metal additive manufacturing. *Addit Manuf* 27:290–304
 85. Takezawa A, To AC, Chen Q, Liang X, Dugast F, Zhang X, Kitamura M (2020) Sensitivity analysis and lattice density optimization for sequential inherent strain method used in additive manufacturing process. *Comput Methods Appl Mech Eng* 370:113231
 86. Takezawa A, Chen Q, To AC (2021) Optimally variable density lattice to reduce warping thermal distortion of laser powder bed fusion. *Addit Manuf* 48:102422
 87. Pellens J, Lombaert G, Michiels M, Craeghs T, Schevenels M (2020) Topology optimization of support structure layout in metal-based additive manufacturing accounting for thermal deformations. *Struct Multidiscip Optim* 61:2291–2303
 88. Chen Q, Liu J, Liang X, To AC (2020) A level-set based continuous scanning path optimization method for reducing residual stress and deformation in metal additive manufacturing. *Comput Methods Appl Mech Eng* 360:112719
 89. Osher S, Sethian JA (1988) Fronts propagating with curvature-dependent speed: algorithms based on Hamilton-Jacobi formulations. *J Comput Phys* 79:12–49
 90. Chen Q, Taylor H, Takezawa A, Liang X, Jimenez X, Wicker R, To AC (2021) Island scanning pattern optimization for residual deformation mitigation in laser powder bed fusion via sequential inherent strain method and sensitivity analysis. *Addit Manuf* 46:102116
 91. Li L, Anand S (2020) Hatch pattern based inherent strain prediction using neural networks for powder bed fusion additive manufacturing. *J Manuf Process* 56:1344–1352
 92. Noll I, Bartel T, Menzel A (2021) On the incorporation of a micromechanical material model into the inherent strain method-application to the modeling of selective laser melting. *GAMM Mitteilungen* 44:1–25
 93. Liang X (2020) Modified inherent strain method for predicting residual deformation in metal additive manufacturing. Dissertation, University of Pittsburgh 58:iii

Publisher's Note Springer Nature remains neutral with regard to jurisdictional claims in published maps and institutional affiliations.

Springer Nature or its licensor holds exclusive rights to this article under a publishing agreement with the author(s) or other rightsholder(s); author self-archiving of the accepted manuscript version of this article is solely governed by the terms of such publishing agreement and applicable law.